UNIVERSITY of PENNSYLVANIA

ELECTRICAL ENGINEERING DEPARTMENT

14-th Quarterly Report

BIOMORPHIC NETWORKS FOR ATR AND HIGHER-LEVEL PROCESSING

Period covered: 4/01/98 - 7/01/98

Submitted to:
Office of Naval Research
W. Miceli - Scientific Officer

Grant No: N00014-94-0931

Prepared by:

Nabil H. Farhat, Principal Investigator

July 1998

The Moore School of Electrical Engineering
Department of Electrical Engineering
University of Pennsylvania
Philadelphia, PA 19104-6390
215-898-5882
215-573-2068-FAX
e-mail: farhat@pender.ee.upenn.edu

July 1, 1998

Scientific Officer Code: 4414
W.J. Miceli
Office of Naval Research
Ballston Tower One
800 North Quincy Street
Arlington, Virginia 22217-5660

Re: Grant Not: N00014-94-0931

Dear Dr. Miceli,

Please find enclosed the fourteenth quarterly report for the referenced grant. I appreciate ONR's support of this research.

Sincerely,

N. Farhat
Professor

C.C. Distribution List
/Enclosure

REPORT DOCUMENTATION PAGE

Form Approved
OMB No. 0704-0188

1. AGENCY USE ONLY (Leave blank)	2. REPORT DATE	3. REPORT TYPE AND DATES COVERED
	January 10, 1998	Quarterly - 01/01/98 - 4/01/98

4. TITLE AND SUBTITLE

BIOMORPHIC NETWORKS FOR ATR AND HIGHER-LEVEL PROCESSING

5. FUNDING NUMBERS

N00014-94-0931

6. AUTHOR(S)

Nabil H. Farhat

7. PERFORMING ORGANIZATION NAME(S) AND ADDRESS(ES)

Nabil H. Farhat
Electrical Engineering Department
University of Pennsylvania
200 South 33rd Street
Philadelphia, PA 19104-6390

8. PERFORMING ORGANIZATION REPORT NUMBER

14

9. SPONSORING/MONITORING AGENCY NAME(S) AND ADDRESS(ES)

Scientific Officer Code: 4414
William Miceli
Office of Naval Research
Ballston Tower One
800 North Quincy Street, Arlington, Virginia 22217-5660

10. SPONSORING/MONITORING AGENCY REPORT NUMBER

11. SUPPLEMENTARY NOTES

12a. DISTRIBUTION/AVAILABILITY STATEMENT

DISTRIBUTION STATEMENT A
Approved for public release;
Distribution Unlimited

12b. DISTRIBUTION CODE

13. ABSTRACT (Maximum 200 words)

14. SUBJECT TERMS

15. NUMBER OF PAGES
8

16. PRICE CODE

17. SECURITY CLASSIFICATION OF REPORT	18. SECURITY CLASSIFICATION OF THIS PAGE	19. SECURITY CLASSIFICATION OF ABSTRACT	20. LIMITATION OF ABSTRACT
UNCLASSIFIED	UNCLASSIFIED	UNCLASSIFIED	

During the period of this report a document entitled: "Biomorphic Networks: Approach to invariant feature extraction and segmentation for ATR" was completed. It consolidates and describes earlier and more recent efforts in this aspect of our research. A copy of the document is attached to serve as the quarterly report. A paper with the same title is scheduled for presentation at SPIE'98, San Diego this July.

Publications during this period:

1. N.H. Farhat, "Biomorphic Dynamical Networks for Cognition and Control", Journal of Intelligent and Rototic Systems, Vol. 21, pp. 167-177, (1998). (copy attached)

Biomorphic networks: Approach to invariant feature extraction and segmentation for ATR*

A. S. Baek and N. H. Farhat
Department of Electrical Engineering
University of Pennsylvania
Philadelphia, PA 19104

ABSTRACT

Invariant features in two dimensional binary images are extracted in a single layer network of locally coupled spiking (pulsating) model neurons with prescribed synapto-dendritic response. The feature vector for an image is represented as invariant structure in the aggregate histogram of interspike intervals obtained by computing time intervals between successive spikes produced from each neuron over a given period of time and combining such intervals from all neurons in the network into a histogram. Simulation results show that the feature vectors are more pattern-specific and invariant under translation, rotation, and change in scale or intensity than achieved in earlier work. We also describe an application of such networks to segmentation of line (edge-enhanced or sihlouette) images. The biomorphic spiking network's capabilities in segmentation and invariant feature extraction may prove to be, when they are combined, valuable in Automated Target Recognition (ATR) and other automated object recognition systems.

Keywords: Spiking neural networks, biomorphic neuron, feature extraction, distortion invariance, segmentation, automated object recognition

1. INTRODUCTION

Invariant feature extraction plays a central role in designing automatic object recognition systems, whose applications permeate a diverse range of fields that include radar, sonar, optical character recognition, autonomous vision machines for use in space exploration, robotics, and manufacturing. The human visual system recognizes objects remarkably well from two dimensional images cast on the retina, even when these images are distorted by various factors such as change in the distance and orientation of the object, light illumination level, shading and background clutter. Understanding and duplicating this exceptional invariant recognition ability of the visual system is valuable for successful development of advanced automatic target recognition (ATR) systems.

To this end artificial neural network models based on neuronal firing rate have been explored and applied in the past, with various degrees of success, to both the feature extraction and the recognition aspects of ATR [1]. It is however becoming increasingly clear that the temporal aspects of brain function manifested in the spiking nature of neural activity and the relative timing of spikes may play an important role in distortion invariant feature-extraction, feature-binding and other higher-level brain functions.

In this paper we will present methods for invariant feature extraction and image segmentationin using a network of biomorphic spiking neurons that extends and improves on earlier published work. Invariant features in two dimensional binary images are extracted in a single layer network of locally coupled spiking (pulsating) neurons that include synapto-dendritic processing. The feature vector for an image emerges as invariant structure in the aggregate histogram of interspike intervals, which is formed by computing time intervals between successive spikes produced from each neuron over a given period of time and combining such intervals from all neurons in the network into a histogram. The simulation results presented here show that the feature vectors are object-specific and highly invariant under translation, rotation, and change in scale or intensity. The results suggest that the combined process

* Based in part on an oral presentation given given at the 1997 OSA Annual Meeting, Long Beach, CA Oct. 1997.

of the segmentation and feature extraction from segmented images may provide useful basis in designing ATR and other autonomous recognition systems.

Current techniques for distortion invariant pattern recognition use integral transforms, algebraic moments, or perceptron-like neural networks with learning algorithms [2]. These techniques demand, however, extensive computational resource and are susceptible to spatial noise in the input image. Recently, a novel pulse-coupled neural network, which could generate invariant signatures of images of simple canonical patterns under translation, rotation, scale and intensity changes, was described in [3]. Although our method is an extension of this earlier work in that it also uses a pulse-coupled neural network and employs concepts developed in [3] and [4], there is a fundamental difference between the network dynamics in the two methods. The method presented in [3] is based on the cortical model of synchronization of neural temporal activity developed in [4] but uses moderate-to-weak linking strengths to induce phase-locked firing states of neurons. Also in [3], the spatial structure of the test patterns (a cross and a tee), made of blocks with each block containing 11×11 pixels and a distinctive gray-scale intensity level, was encoded in the phase-locking pattern of output spikes from neurons. In contrast, the method described here is less "corticomorphic". It is based on firing rate encoding, which is predominantly observed in sensory nervous systems, rather than phase-locking, and is suited for processing binary line images. This different encoding scheme arises, as explained below, from the opposite relationship between the time constants of the synaptic response function and the membrane potential (pulse generator) that we use as compared to [3]. As a result, the method appears to produce invariant feature vectors that are more input pattern specific than in [3], which is a desirable prerequisite for accurate classification. Also, its ability to extract invariant features of binary line images is an attractive attribute because edge-enhancement and line extraction are standard operations in pattern recognition.

In Section 4, we demonstrate the ablity of the spiking neural networks in segmentation of line images (eg. silhouettes or edge enhanced images) of model objects. Once characteristic segments of a line image are obtained, each segment may be processed by a biomorphic spiking network, similar to the one described in Section 2, to produce a set of histograms of interspike intervals, which contain invariant features that are specific to the line image. The resulting set of invariant features, which belong to the respective features of the image, can then be regarded as a composite invariant feature vector that represents the entire line image.

2. THE NETWORK

In the invariant feature extraction system presented here, a basic image that consists of a 12×12 binary pixel array is fed to a single layer network that consists of spiking neurons arranged in the 12×12 array format. The model neuron used in the network is of the integrate-and-fire (I&F) variety , similar to that used in [3]-[5], and is regarded as biomorphic in that it contains a simplified model of the dendritic-tree processing in biological neurons, as explained below.

The dynamics of the neuron can be summarized as follows, refering to Fig.1. When the exponentially rising membrane potential, $\Delta V_m(t)$, of the neuron at (i,j) reaches the time-varying threshold, $V_{ij}^{th}(t)$, it instantaneously drops to the resting membrane potential V_{rest} and at the same time a spike (action potential) is generated [6]. The time-varying threshold is represented as

$$V_{ij}^{th}(t) = V_0 - U_{ij}(t) \tag{1}$$

where V_0 is constant and $U_{ij}(t)$, as defined below in Eqn. (3), is a signal that results from the joint actions of synaptic inputs and the intensity of the image. This process of exponential rise and instantaneous drop of the membrane potential repeats, generating successive spikes whose timing is modulated by the threshold voltage. Note that lowering the threshold causes the neuron to fire faster, because it takes less time to build the membrane potential from the resting potential to the threshold.

In an effort to emulate the signal processing that occurs in the dendritic tree of biological neurons, the model neuron is given a simplified homogeneous synapto-dendritic response function modeled as an impulse response function, which approximates the change in membrane potential (depolarization) at the neuron's hillock (i.e, the site of output spike generation), in response to a single spike on its dendritic tree. We use an exponentially decaying function for the synapto-dendritic response, given by

$$h(t) = h_o \exp(-t/\tau) \tag{2}$$

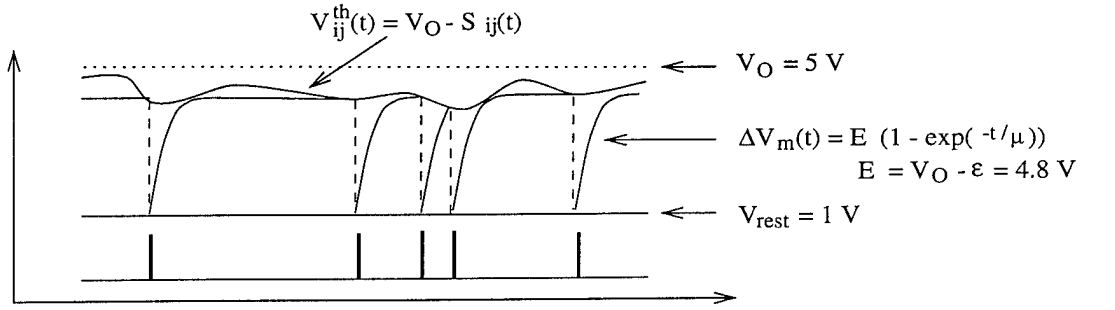

$S_{ij}(t) = I_{ij}(1 + \beta P_{ij}(t))$

$P_{ij}(t) = ST_{ij} * h(t)$

$h(t) = h_o \exp(-t/\tau)$

$\mu = 1$ msec (membrane time constant)

$\tau = 12$ msec (synapto-dendritic time constant)

Figure 1. The dynamics of the biomorphic spiking neuron and parameters used in numerical simulations.

where τ is the time constant of the response. Also, the model neuron in the network receives the intensity value of the image at the corresponding coordinates, which modulates the signal produced from synaptic inputs in a nonlinear manner similar to that in [3] and [4], as further explained below.

Using the same notation as in [3] and [4], the signal, $U_{ij}(t)$, which is produced from a nonlinear combination of the external input and synaptic inputs, is determined by Eqn. (3) with i and j representing the coordinates of both the pixel and the neuron in the 12×12 array. The signal $P_{ij}(t)$, as defined in Eqn. (4), is a convolution of the synapto-dendritic response function and the input spike train impinging on the neuron at (i, j). The input spike train is represented below as a sum of delta functions with m and n representing the coordinates of the sending neuron and k representing the spike generation time.

$$S_{ij}(t) = I_{ij} \times (1 + \beta P_{ij}(t)) \tag{3}$$

$$P_{ij}(t) = ST_{ij} * h(t) \tag{4}$$

$$ST_{ij}(t) = \sum_{mnk} \delta(t - t_{mn}^k) \tag{5}$$

The signal $S_{ij}(t)$ modulates the threshold voltage of the neuron at (i, j), as shown in Eqn. (1), and this will determine the firing times. The departure of the membrane potential V_m from the resting value V_{rest} can be expressed as:

$$\Delta V_m(t) = E(1 - \exp(-\frac{t}{\mu})) \tag{6}$$

$$E = V_o - \epsilon \tag{7}$$

where V_o and ϵ are given values of 5 and 0.2 volts, respectively in the simulations below. When a spike is elicited, the membrane potential V_m instantaneously drops to the resting potential V_{rest} and begins to rise exponentially towards the time-varying threshold, $V_{ij}^{th}(t)$ as depicted in Fig.1.

Attention is drawn to the relationship between the time constant μ of the exponential membrane build-up and the time constant τ of the synapto-dendritic response function. In contrast to the practice in [3] in which the time constant of the synapto-dendritic response is shorter than that of the membrane dynamics (referred to as pulse generator in [3]), the time constant τ of the synapto-dendritic response here is longer than the time constant μ of the membrane potential build-up. This alteration of the relation between the time constants produces a markedly different network behavior in that the prolonged synapto-dendritic response causes slow depressions in the threshold of a neuron, affecting its firing rate. In our simulations, the time constant τ of the synapto-dendritic response function is $12msec$, while that of the membrane potential build-up is $1msec$. In contrast the time constants in [3] are 1 for synaptic response and 5 for the membrane threshold (pulse generator) (units were not specified).

Another important feature of the model neuron used here, which is adopted from [3] and [4], is the nonlinear combination of the extrinsic input I_{ij} and the intrinsic input from other neurons $P_{ij}(t)$, as defined by Eqn. (3). The

pixel intensity of the image modulates the signal produced from synaptic inputs. The strength of the modulation is controlled by the constant β. Especially, when I_{ij} is zero, the neuron at (i, j) can not fire, because $U_{ij}(t)$ then becomes zero, according to Eqn. (3), and the neuron operates in the sub-threshold mode (the membrane potential saturates before reaching the threshold voltage). The value of $I_{ij} = 0$ effectively nullifies any effects of synaptic inputs on the threshold, forcing the neuron to be "silent". This nonlinear operation is similar to the biological situation in which inhibitory inputs proximal to the soma (cell body) may effectively nullify excitation by inputs on distal synapses [7]. In a complex morphological dendritic tree, this type of a selective AND-NOT like operation can effectively decouple subunits of the tree.

The network architecture used is shown in Fig. 2(a). The neurons are arranged in a 12×12 array and a sample neuron in the lower right side of the array is depicted showing its synaptic connections from its 8 nearest neighboring neurons. Interspike intervals of the spike train from each neuron are computed in the local interspike interval analyzers and the results are combined to form the aggregate interspike interval histogram. Shown in Fig. 2(b) is the schematic of an isolated neuron with the two types of inputs, the instrinsic synaptic inputs from the neighboring neurons and the extrinsic pixel intensity value from the image.

3. SIMULATION RESULTS

The simulations results are shown in Figs. 3, 4, and 5 with the input images and the associated aggregate (interspike interval histograms) ISIHs shown in the left and the right columns, respectively. Figure 3(a) shows the simulation result with the original image of the tee. The input image in Fig. 3(b) is a scaled, 90-degree rotated, and translated version of the original tee image. Figures 3(c) and (d) show the input images of the cross and the associated output ISIHs. Already from these simulations, one can clearly see the differences between the histograms produced from the tee images and from the cross images and the invariance of the histograms with image distortions. In Figs. 4(a) and (b) for a rectangle, the histograms are drastically different from the previous cases of the tee and the cross, highlighting the pattern-specificity, and the invariance is well retained for the rectangle in the distortions of scale, rotation, and translation. As reader might have noticed, the angles used in the simulations for the rotational invariance are confined to the multiples of 90 degrees, due to the limited spatial resolution. At higher spatial resolution, this restriction on the rotation angle can be relaxed and the rotation invariance for in-between angles will be achieved. The invariance with scale for a triangle is shown in Fig. 4(c) and (d). We have also examined invariance with intensity for the triangle, as demonstrated in Figs. 5 (a) and (b). The uniform intensity of the triangle used for Figs. 5 (a) is 10 percent higher than that used for Figs. 5 (b). The characteristic form of the histogram for the triangle is seen to be retained but experiences a shift towards lower time interval region. The shift comes from the fact that the higher uniform image intensity lowers the thresholds of the neurons, raising the firing rate. On a relevant note, we have an indication from later simulations that using a synapto-dendritic response function that is more biomorphic, i.e., approximates the biological response more accurately [8], results in higher invariance to the distortions, especially the intensity change. Results from these simulations are not reported here due to space limitation.

The invariant structure in ISIH is closely related to characteristic local features of the input pattern. For instance, the main feature of the triangle is the three corners. The neurons residing in these corners of the triangle and the vicinities have higher firing rates that are responsible for invariant structure in the ISIH, since they are connected to more neighboring neurons with higher activity than the neurons in the middle of edges. Such analysis carried out by the network is meaningful for syntactical information processing in that the input image can be implicitly segmented into sections that contain characteristic structural information. It is, however, important to remember that due to the convoluted nature of inter-neuron interactions through pulse-coupling, the invariant structure in the ISIH is also affected indirectly by activity of neurons that are beyond the nearest neighboring connections. Although this distal interaction is much weaker than the local interaction, it still seems to take a part in determining the shape of the ISIH.

4. SPIKING NETWORK FOR SEGMENTATION

A preliminary study of the ability of biomorphic spiking networks to segment line images (i.e., silhouettes or edge enhanced images) of model objects was carried out. The representative results given next suggest that combining spiking networks for segmentation with spiking networks for invariant feature extraction may offer a viable approach for generating invariant features for extended objects.

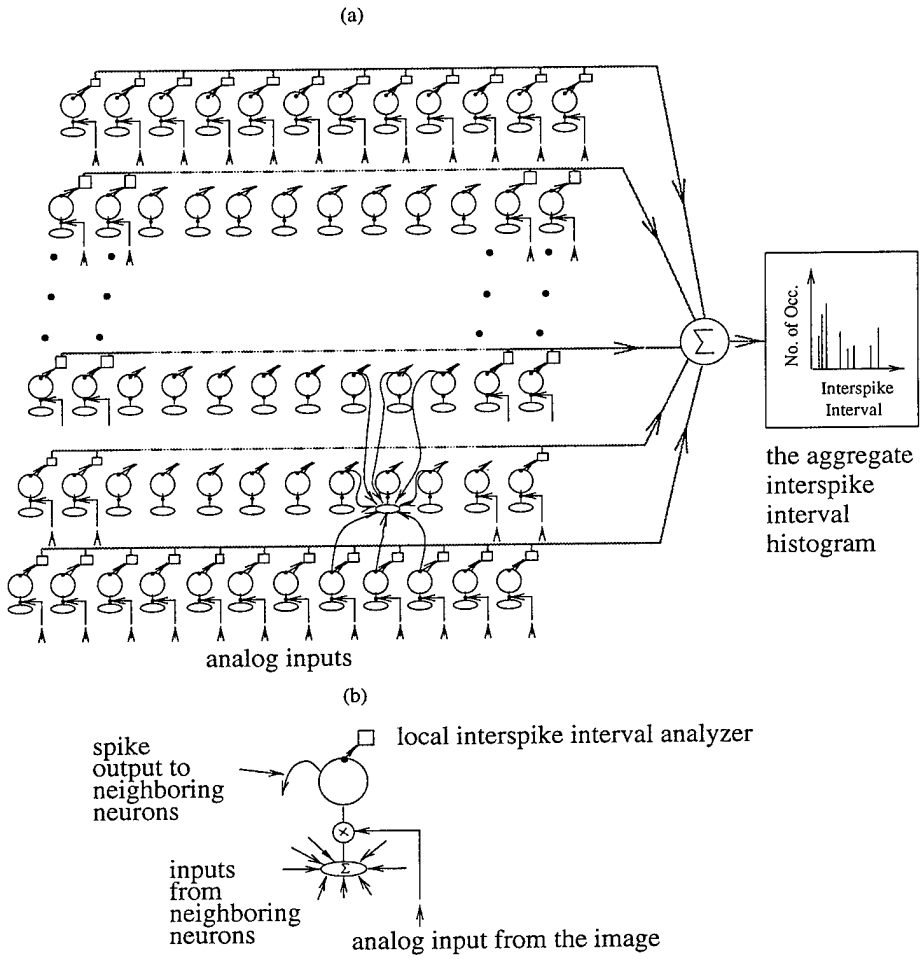

Figure 2. (a) Schematic of the network arranged in the $N \times N$ array. A set of exemplar synaptic connections of a neuron from its eight neighboring neurons is shown in the lower right side of the array, with the cursive lines representing the connections. Interspike intervals from each neuron are computed in the local interspike interval analyzer and sent to the aggregate interspike interval histogram. (b) Schematic of the neuron with two types of inputs: synaptic inputs from its neighboring neurons and an analog input of the image intensity at the neuron's location. The two types of the inputs are combined in a multiplicative manner to produce a signal that influences the timing of action potential generation and therefore the spiking output to the synaptically connected neurons.

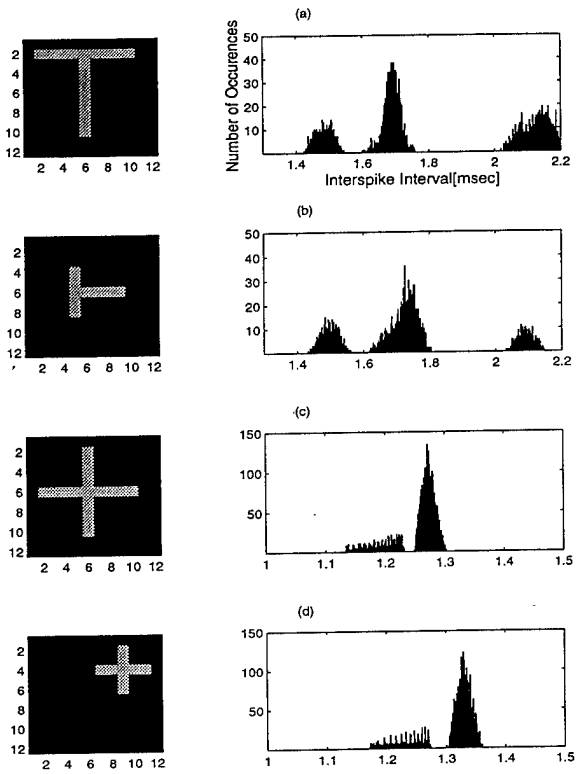

Figure 3. Simulation results with the tee and the cross demonstrating invariance with translation, rotation, and scale. The input images and the aggregate (interspike interval histograms) ISIHs from simulations are shown in the left and the right column, respectively. (a) The tee image, (b) A 90-degree rotated, scaled, and translated version of the tee in (a), (c) The cross image, (d) A scaled and translated version of the cross in (c). The time resolution of the ISIHs is 0.001 msec.

In order to obtain the input line images, test objects (two types of model aircrafts and one tank) were photographed using a CCD camera, then digitized and saved in gray-scale in 400×400 pixel format. Examples of such gray scale images are shown in Figs. 6(a), 7(a), and 8(a). The gray-scale images were then binarized and edge-detected to produce the line images as shown in Figs. 6(b), 7(b), and 8(b). In producing the line image, if the gray-scale image is smaller than 400×400, we padded the remaining pixels with zero intensity to maintain a consistent image size. Then, the line image was fed into the biomoprhic neural network, which has the same dimensions as those of the input image format. The neurons of the network used here employed an alpha function [8] for the synapto-dendritic response in place of the exponential function given by Eqn.3. Note that the neurons which receive zero intensity from the image do not fire, because the signal $S_{ij}(t)$ in Eqn. (3) is zero for all such neurons.

Figures 6(c), 7(c), and 8(c) present the simulation results with the neurons' firing rates given in gray scale. the synaptic weight matrix used in the simulation was circularly symmetric with a radius of 21 pixels, and had a uniform excitatory synaptic weight of one within the circle. In these plots, the brighter pixels indicate higher firing rates for the neurons located in those spots. We then varied a threshold firing rate and plotted only those pixels whose firing rate is above the threshold, as shown in Figs. 6(d), 7(d), and 8(d) to segment the line images into characteristic segments each of which can potentially be represented by an invariant ISIH with the aid of a network similar to that described in Section 2. The pronounced features in Fig. 5 6(d) are the engines in the rear, the tips of the wings, the angels at the functions of the wings and the main body, while in Fig. 7(d) they are the tail, the engines and the gun barrels on the wings, and the front tip. In Fig. 6(d), the biomoprhic network extracted (segmented) the most characteristic feature of tanks, the nozzle.

Figures 9 and 10 show the invariance of segmenting the line images of Aircrafts 1 and 2 under translation, rotation, and change of scale. The simulation results using images of Aircrafts 1 and 2 are shown with the input edge-enhanced images given on the left and the simulation results showing neurons with firing rates above a certain

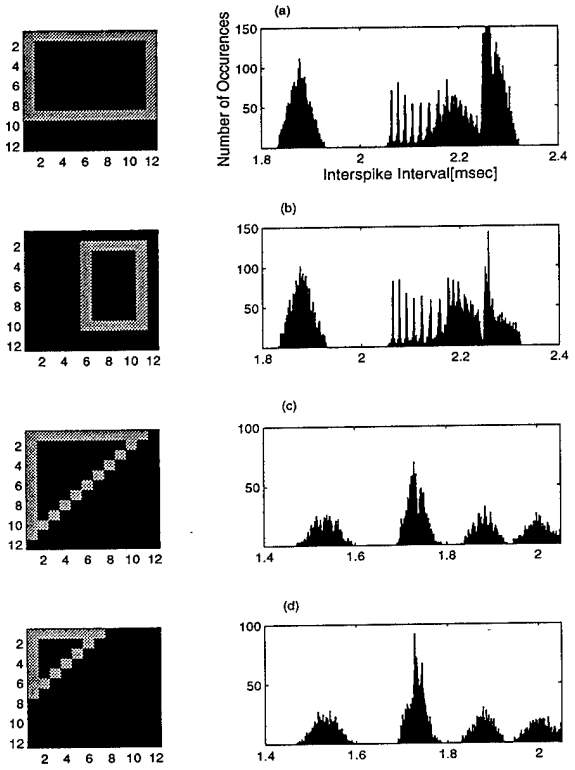

Figure 4. Simulation results with the rectangle and the triangle demonstrating invariance with invariance of translation, rotation, and scaling. The input images and the aggregate ISIHs from simulations are shown in the left and the right columns, respectively. (a) The rectangle image, (b) A 90-degree rotated, scaled, and translated version of the rectangle in (a), (c) The triangle image, (d) A scaled version of the triangle in (c).

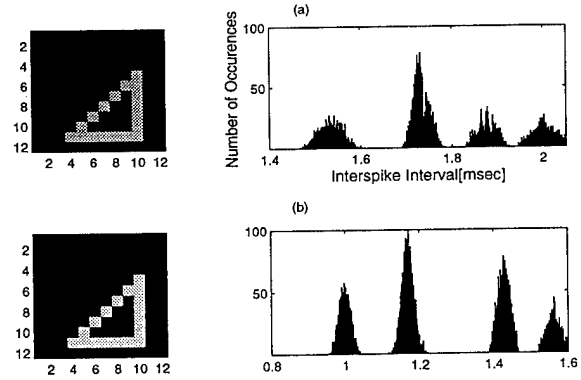

Figure 5. Simulation results with the triangle for intensity invariance. The input images and the aggregate ISIHs from simulations are shown in the left and the right columns, respectively. (a) The triangle image, (b) The triangle image with uniform intensity increased by 10 percent.

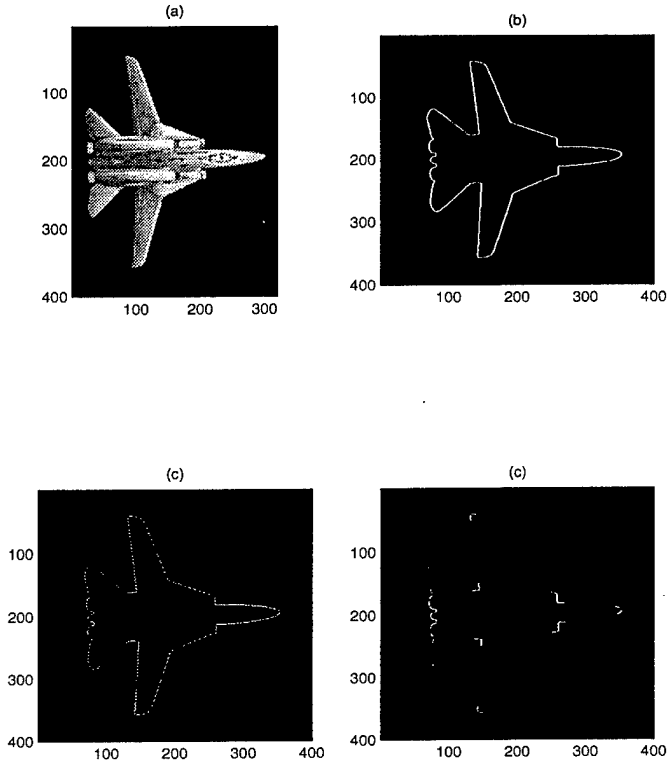

Figure 6. Segmentation of gray scale image of model Aircraft 1. (a) Gray scale image of model Aircraft 1, (b) The line image of the gray scale image in (a), (c) Firing rates of the biomorphic neurons with the brightest pixels representing the highest firing rates, (d) Plot of firing rates above a prescribed threshold. The plot shows characteristic segments of the aircraft, each of which maybe further analyzed by a feature extracting network to represent it by an invariant ISIH. The invariant histograms of the segments form an "invariant set", which can be used to represent the object and serve as an input to an ATR system.

threshold in the right. In these simulations, the circularly symmetric synaptic weight matrix has two concentric circles with radii of 48 and 51 pixels. The matrix elements inside the inner circle with radius of 48 pixels have a uniform excitatory synaptic weight of one, while those between the inner and the outer circles have a uniform inhibitory synaptic weight of negative one. We observed that the circularly symmetric weight with a large radius produces better rotation invariance. When the radius decreases, the synaptic matrix delineated over the rectangular array loses circular symmetry and becomes a square, due to the spatial resolution limitation. Also in the simulations shown in Figs. 9 and 10, the inhibitory weight is used to balance off the excitatory synaptic connections and avoid saturation of neurons' firings. The simulation results show that robust invariance under translation, rotation, and scale, is achieved.

In the above simulations involving model objects, as well as in the previous examples involving canonical objects, the geometrical complexities are encoded in firing rates of the neurons that reside in the corresponding locations. As we have seen, sections of the images that contain complicated structure become pronounced in the firing rate plot.

5. CONCLUSIONS

We have described a spiking neural network that can extract invariant feature vectors of two dimensional binary line images based on firing rate encoding rather than encoding by phase-locking described in [3]. The difference seems to lead to feature vectors or signatures for binary line images that are more pattern-specific and invariant under translation, rotation, and change in scale or intensity than achieved in [3]. Also the simpler neuronal and network structures used here can be advantageous in hardware implementation for real-time processing.

A preliminary study of the ability of biomophic spiking networks to segment line images (i.e., silhouettes or edge enhanced images) of model objects was also carried out. The results suggest that the the combined processing of

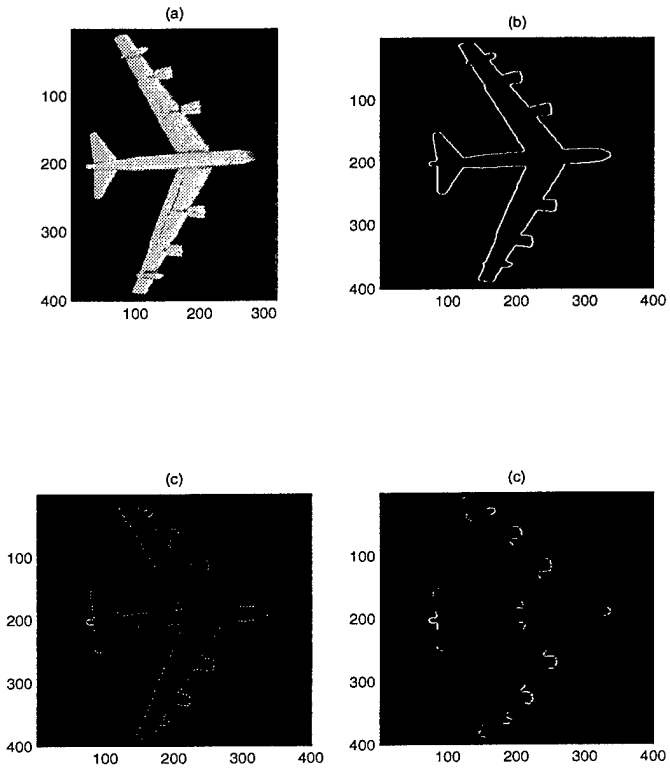

Figure 7. Segmentation of gray scale image of model Aircraft 2. (a) Gray scale image of model Aircraft 2, (b) The line image of the gray scale image in (a), (c) Firing rates of the biomorphic neurons with the brightest pixels representing the highest firing rates, (d) Plot of firing rates above threshold. The plot shows characteristic segments of the aircraft.

segmentation and feature extraction, each peformed by respective spiking networks, may provide a viable approach for generating invariant feature vectors for extended objects, which is worthy of further investigation.

ACKNOWLEDGMENTS

This research was supported by the Office of Naval Research under grant no. N0001-94-1-093P01 and in part by NASA Graduate Student Researchers Programs for one of us (A. Baek).

REFERENCES

1. H. Babri, "Neurodynamic networks for recognition of radar targets", Ph.D. dissertation, University of Pennsylvania, 1992.
2. J. Wood, "Invariant pattern recognition," *Pattern Recognition* **29**, pp.1, 1996.
3. J. L. Johnson, "Pulse-coupled neural nets: translation, rotation, scale, distortion, and intensity isgnal invariance for images," *Appl. Opt.* **108**, pp.6239, 1994.
4. R. Eckhorn, H. J. Reitboeck, M. Arndt, and P. Dicke, "Feature linking via synchronization among distributed assemblies: simulations of results from cat visual cortex," *Neural Comput.* **2**, pp.293 (1990).
5. N. H. Farhat, S. Y. Lin, and M. Eldefrawy, "Complexity and chaotic dynamics in a spiking neuron embodiment," *Proc. SPIE* **CR55**, pp.77, 1994.
6. J. G. Nicholls, A. R. Martin, and B. G. Wallace, *From Neuron to Brain*, Sinauer, Sunderland, MA, 1992.
7. C. Koch and T. Poggio, Trends in Neuroscience **3**, pp.455, 1983.
8. P. S. Anton, R. Granger, and G. Lynch, in *Single Neuron Computation* T. McKenna, J. Davis, and S. F. Zornetzer, eds. pp. 291, Academic, San Diego, CA, 1992d.

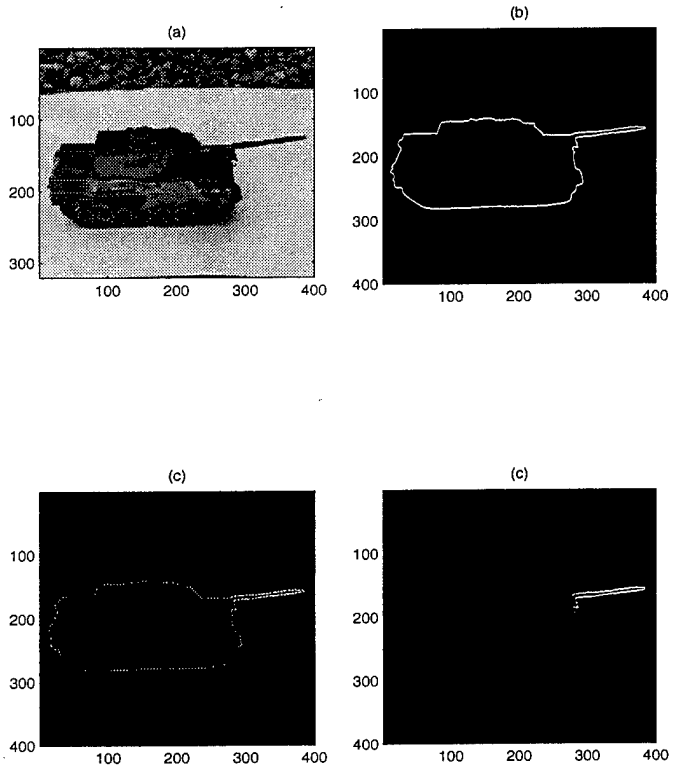

Figure 8. Segmentation of gray scale image of a model tank. (a) Gray scale image of a model tank, (b) The line image of the gray scale image in (a), (c) Firing rates of the biomorphic neurons with the brightest pixels representing the highest firing rates, (d) Plot of firing rates above a threshold. The plot shows a characteristic segment of the tank, the nozzle.

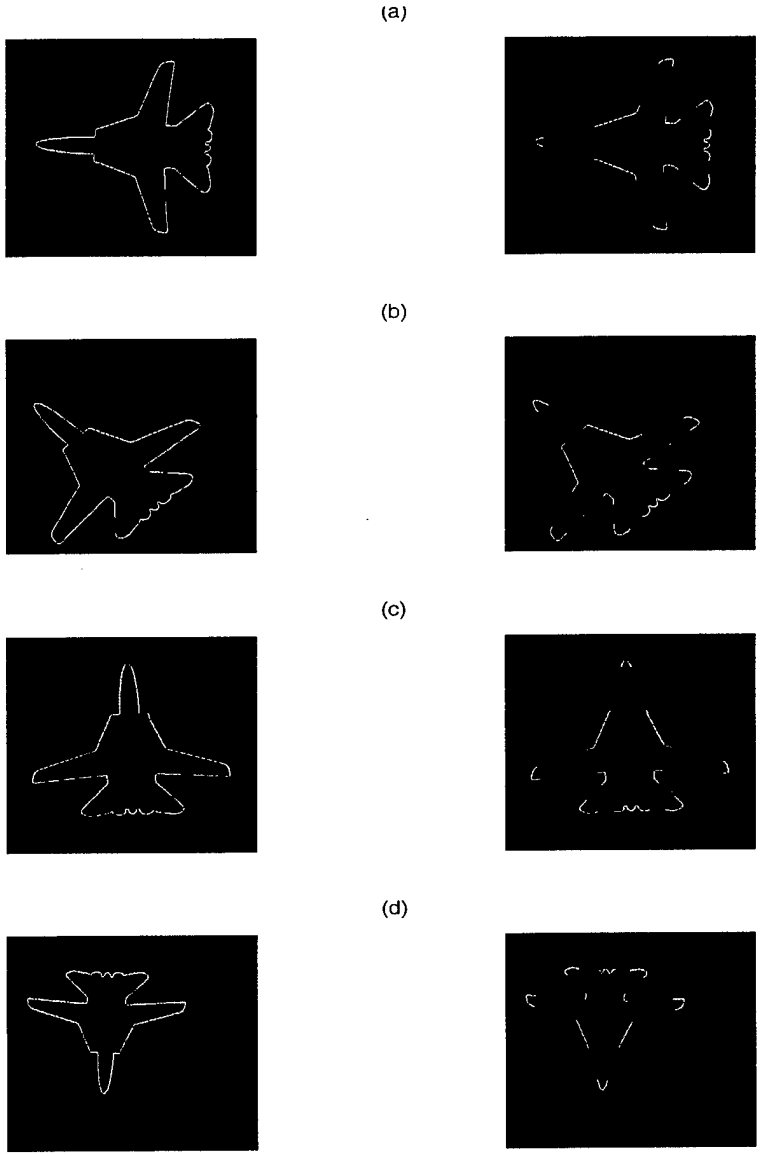

Figure 9. Invariant segmentation of edge-enhanced images of model Aircraft 1. The input images and the invariant segmented image formed by thresholding firing rates of the neurons are shown in the left and the right columns, respectively. (a) Segmentation of the original edge enhanced image of model Aircraft 1, (b) Segmentation of a 45-degree rotated and translated image of the original image shown in (a), (c) Segmentation of a 90-degree rotated image of the original, (d) segmentation of a 90-degree rotated, 80-percent scaled, and translated image of the original.

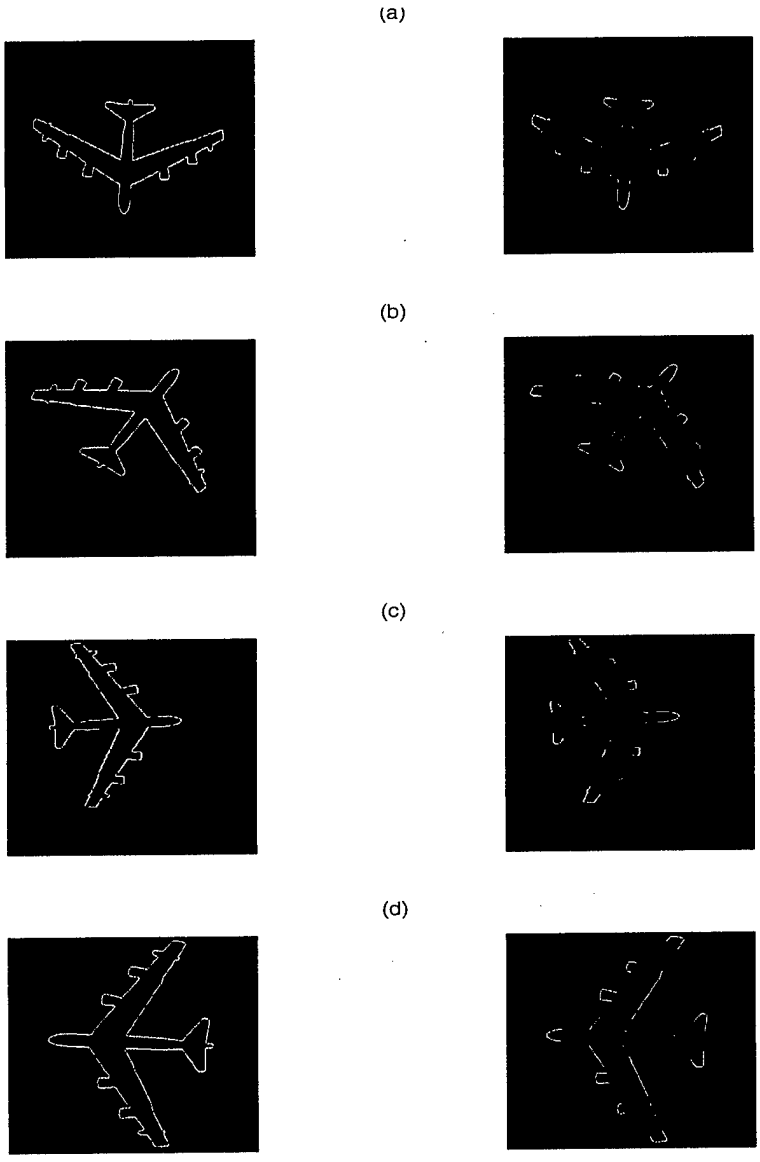

Figure 10. Invariant segmentation of edge-enhanced images of model Aircraft 2. The input images and the invariant features derived from thresholding firing rates of the neurons are shown in the left and the right columns, respectively. (a) Segmentation of the original edge enhanced image of model Aircraft 2, (b) Segmentation of a 135-degree rotated and translated image of the original image shown in (a), (c) Segmentation of a translated image of the original, (d) Segmentation of a 90-degree rotated and 120-percent scaled image of the original. Notice a change of scale of a segment will not affect the ability of a spiking network of the type described in Section 2 to extract an invariant IHIS.

Journal of Intelligent and Robotic Systems **21:** 167–177, 1998.

Biomorphic Dynamical Networks for Cognition and Control

N. H. FARHAT
Electrical Engineering Department, University of Pennsylvania, 200 South 33rd Street, Philadelphia, PA 19104-6390, USA; e-mail: farhat@pender.ee.upenn.edu

(Received 21 July 1997; accepted: 23 September 1997)

Abstract. Advances in understanding the neuronal code employed by cortical networks indicate that networks of parametrically coupled nonlinear iterative maps, each acting as a bifurcation processing element, furnish a potentially powerful tool for the modeling, simulation, and study of cortical networks and the host of higher-level processing and control functions they perform. Such functions are central to understanding and elucidating general principles on which the design of biomorphic learning and intelligent systems can be based. The networks concerned are dynamical in nature, in the sense that they "compute" not only with static (fixed-point) attractors but also with dynamic (periodic and chaotic) attractors. As such, they compute with diverse attractors, and utilize transitions (bifurcation) between attractors and transient chaos to carry out the functions they perform. An example of a dynamical network, a *parametrically coupled net of logistic processing elements*, is described and discussed together some of its behavioural attributes that are relevant to elucidating the possible role for coherence, bifurcation, and chaos in higher-level brain functions carried out by cortical networks.

Key words: neuronal code, netlets, logistic map, dynamical computing, coherence, bifurcation, chaos, collapse into low-dimensional attractors.

1. Introduction

Meaningful progress in learning and intelligent systems is difficult without ability to model and simulate cortical dynamics and the way cortical networks carry out the amazing cognitive and control functions we humans seem to do so effortlessly well while coping and learning in a complex environment. The cortex, also believed to be the site of conciousness and all higher-level thought processes, is fundamentally a high-dimensional nonlinear dynamical system. It is well known that a dynamical system of dimension greater than two ($N \geqslant 3$) can exhibit in its state-space, depending on the range of its control parameters, all three types of primary attractors: fixed-point, periodic, and chaotic. Attractor type neural networks in use today to model brain function, rely entirely on point-attractors in their operation. Therefore they can not perform any higher-level cortical functions that might depend on periodic or chaotic attractors or on bifurcations between attractors. To gain insight in cortical dynamics and in the general principles underlying learning and intelligence, one needs to develop a new class of neural net models capable of "computing" with diverse attractors,

and elucidate the roles of coherence (periodicity, synchronicity, phase-locking), bifurcation, complexity,, and chaos in the kind of analog "computations", and autonomous learning they may carry out. To do this meaningfully, one needs to consider one of the most fundamental questions in neuroscience and brain research today, namely the nature or identity of the *neuronal code*, i.e., the way the cortex deciphers and encodes information as it carries out cognitive, learning, and control functions. An attempt at elucidating the neuronal code and how it suggests that cortical networks may be modeled, simulated, and studied with the help of parametrically coupled nets of logistic processing elements is given in Section 2. This is followed in Section 3 by description of some of the more interesting behavior we have observed in simulations carried out with such a network under uniform global coupling and external stimulus with spatio-temporal input. It is found that such networks have the capacity to "self-anneal" or collapse into stimulus (input) dependent periodic (period-m) attractors following a transient "chaotic" period during which the network searches its state-space for an associated dynamic attractor of low dimension. The network accepts naturally both time-varying or stationary input patterns. Moreover we find that the use of activity dependent nonlinear quantized coupling strengths, provides the network with clustering ability wherein, depending on the stimulus pattern, PEs in the network divide into phase-locked groups with the PEs within each group possessing synchronized identical period-m orbits. The value of m is found to be the same for all clusters and the number of clusters gives the dimension of the periodic attractor. The implications of these findings for higher-level processing such as feature-binding and development of novel learning algorithms are briefly discussed.

2. The Neuronal Code

There is much evidence, stemming from anatomical, physiological, and modeling work in favour of the hypothesis that the basic functional unit in the cortex is the *neuronal assembly* or *netlets* (see, for example, Harth et al., 1970; Annios et al., 1970; Usher et al., 1993; Edelman, 1987; van Vreeswijk et al., 1976; Wennekers et al., 1995 and Wennekers and Pasemann, 1996). A netlet consists of randomly interconnected probabilistic neurons, and netlet behavior is described in terms of the activity $A(n) \in [0, 1]$ which represents the fraction of neurons firing at any discrete integer time n (Harth et al., 1970; Annios et al., 1970; Usher et al., 1993). Discrete-time dynamics are justified by refractoriness, and the temporal and spatial fine structure in neuronal activity within a netlet are considered to be of secondary importance and subsumed by netlet dynamics.

We observe that plots of $A(n+1)$ vs. $A(n)$ typically obtained in netlet analysis, (Harth et al., 1970; Annios et al., 1970; Usher et al., 1993), bear remarkable similarity to the return map of the logistic (quadratic) map (Hilborn, 1994). This suggests that the basic functional unit for higher-level cortical processing could

be represented and modeled by a nonlinear iterative map on the unit interval and that networks of *parametrically coupled logistic maps*, resembling those studied also in (Farhat et al., 1996; Perez et al., 1989 and Bertille, 1990), can be used to model and investigate cortical dynamics and therefore higher-level brain function. Similar work on *coupled map lattices* was carried out by Crutchfield and Kaneko (1987) and Kaneko (1993). The state-space orbits or trajectories $X(n)$ produced by the logistic map, like other nonlinear mapping on the unit interval, are known to exhibit periodic (period-m) orbits, chaotic orbits, and bifurcation between them depending on the value of the control or bifurcation parameter μ of the map. The control parameter can be made, for example, as in (Farhat et al., 1996), to be the input or driving signal of the map resulting in a *parametrically driven logistic processing element*. One can expect netlets to behave in a like manner where the activity $A(n)$, analogous to $X(n)$ of the logistic map, would exhibit similar complex orbits. Indeed, such behavior has been observed in some of the netlet models studied (Wennekers and Pasemann, 1996). What can be quite significant, is that periodicity, bifurcation, and chaos can emerge on the driven netlet level despite the well known imprecision of neuronal firing. This picture goes some way towards elucidating the *neuronal code* and the way brain development and evolution succeeded in getting precise (repeatable) higher-level cortical functions from relatively imprecise neural *wetware*. It provides a plausible answer to an important question in neuroscience, namely how coherence, synchronicity, phase-locking, and deterministic chaos can operate on the netlet and cognitive levels despite the imprecise nature of neuronal firing.

Work described in this paper is therefore based on the novel and intriguing preposition that the basic functional unit for higher-level processing in cortical networks can be modeled by a *bifurcation processing element* (PE) like the *parametrically driven logistic map* (Farhat et al., 1995) or any other one-dimensional driven map on the unit interval. The important attribute of such a PE, which distinguishes it from sigmoidal processing elements (sigmoidal model neurons) used extensively in present day neural networks, is the complex way it encodes information it receives in the form of modulation of its control parameter caused by inputs from other PEs in a network. (The behavior of a bifurcation PE is best described by a bifurcation diagram hence the name.) In this scheme, a cortical net of N interacting netlets, each of which made of a large number (hundreds or thousands) of probabilistic neurons, can be simply modeled and simulated by a network of N parametrically coupled bifurcation processing elements. Earlier work (Farhat et al., 1995; Farhat et al., 1994), indicates that bifurcation PEs can be realized in analog hardware by an *integrate and fire* model neuron equipped with a dendritic tree when it is subjected to correlated spike trains at its dendrites that give rise to a periodic activation potential at its hillock. We may have therefore available to us, for the first time, the means for modeling, simulating, and studying cortical networks both in software and hardware. What all this implies,

and can be quite remarkable, is that in simulation studies a net of N bifurcation PEs would effectively be equivalent to $(10^2$ to $10^3) \times N$ cortical neurons.

3. Parametrically Coupled Network of Logistic PEs (The Logistic Net)

The architecture of the logistic net, shown in Figure 1, consists of N parametrically coupled logistic PEs (parametrically driven logistic maps) described by $X_i(n+1) = \mu_i(n)X_i(n)[1 - X_i(n)]$, where $\mu_i(n) \in [0,4]$, and $X_i(n) \in [0,1]$, $i = 1,2,\ldots,N$, together with N auxilliary "sensory" logistic maps described by $X_i^s(n+1) = \mu_i^s X_i^s(n)[1 - X_i^s(n)]$ with $\mu_i^s \in [0,4]$ and $X_i^s \in [0,1]$. The sensory network is used to produce a wide range of spatio-temporal input patterns to drive the network. The network employs nonlinear activity dependent coupling functions between PEs as an abstraction of the possible occurrence of rapid activity dependent modulation of the coupling between netlets.

To loosely incorporate this activity dependent coupling in the network of Figure 1 we use binned or quantized nonlinear coupling functions $B_i^s(X_i^s)$ from the sensory elements to the PEs and $B_{ij}(X_j)$ between the processing logistic elements (the jth and ith elements) respectively. The step-like nature of these binned coupling functions illustrated in Figure 2 allows sudden changes in the coupling strengths between netlets as their activity, represented here by the state variable $X_i(n)$ of the logistic PE, changes. The number of levels (steps) in the binned coupling functions is arbitrarily chosen to be 4. The use of binned coupling is found to lead to the emergence of clustering and to the avoidance of "fragmentation" in network activity. As seen in Figure 2, the binned coupling function $B_{ij}(X_j)$ for example is formed by the intersection of the horizontal lines A, T, C, G and the nonlinear function $g_{ij}(X_j) = 4X_j^{C_{ij}}$, where C_{ij} is a positive real constant that determines the shape of $g_{ij}(X_j)$ and therefore the location of the steps or breakpoints a, b, c. Similar rules apply to $B_i^s(X^s)$.

The binned coupling functions $B_i^s(X^s)$ and $B_{ij}(X_j)$ determine the value of the control parameter $\mu_i(n)$ of the ith PE in the network according to,

$$\mu_i(n) = \varepsilon \mathrm{O}_i^s(n) + \frac{1-\varepsilon}{N} \sum_{j=1}^{N} \mathrm{O}_{ij}(n), \tag{1}$$

where $\mathrm{O}_i^s(n) = B_i^s(X_i^s(n))$ and $\mathrm{O}_{ij}(n) = B_{ij}(X_j(n))$ with $X_i^s(n)$ and $X_j(n)$ being the state variables of the driven sensory and processing logistic maps respectively and ε is a parameter controlling the relative effects of the extrinsic (sensory) and intrinsic (feedback) activity on $\mu_i(n)$. The simulations presented here are for $\varepsilon = 0.5$.

We have carried out (Farhat et al., 1996) a numerical simulation of the logistic net of Figure 1 for $N = 100$ under a variety of stimulus generating vectors $\overline{\mu}^s$. Homogeneous binned coupling, i.e., $C_i^s = C_{ij} = 0.5$, $i,j = 1,2,\ldots,N$, was used because the emphasis was on studying how the network behaves under

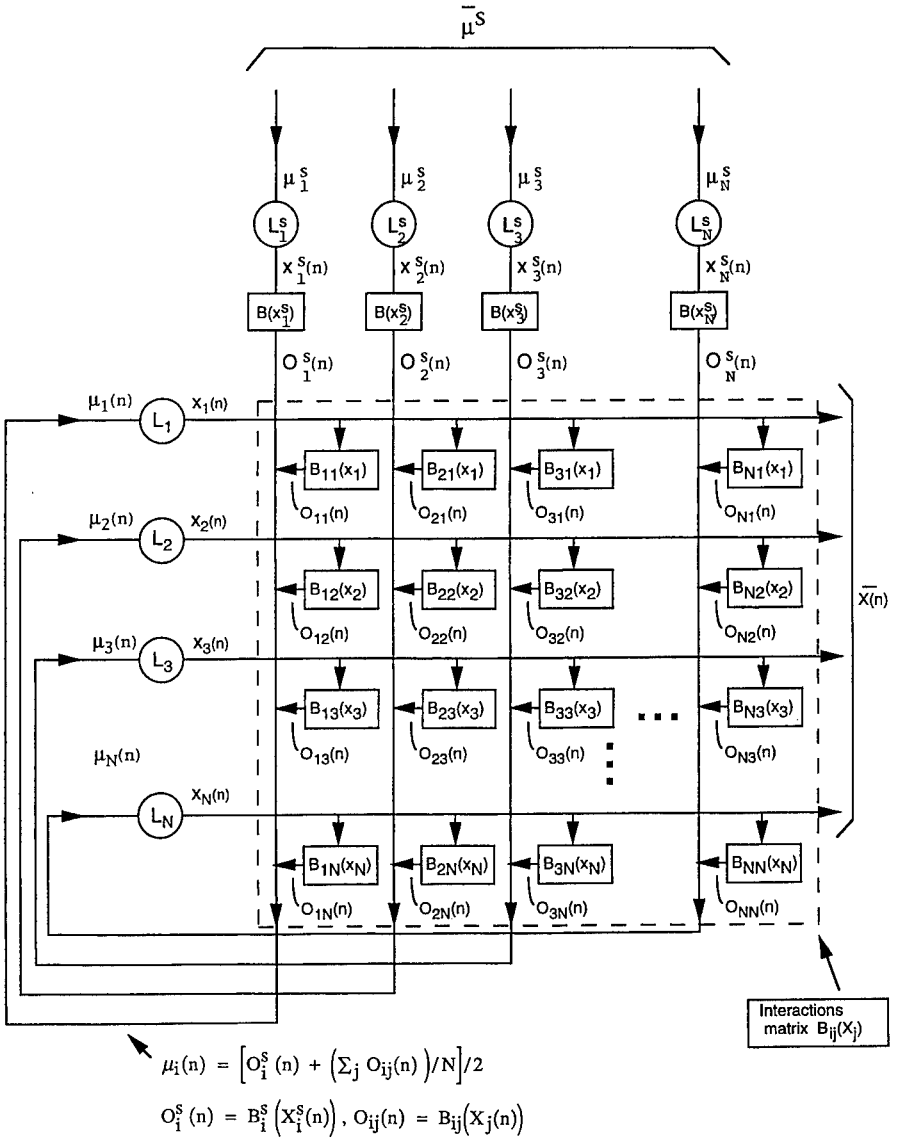

Figure 1. Parametrically coupled net of logistic processing elements (PEs) with binned (quantized) coupling functions.

different types of sensory input patterns and not, in this paper, on adaptation and learning where C_{ij} would be incrementally altered for example by a suitable adaptation algorithm to effect learning. In the simulations described here, all logistic PEs in the net were initiated from the same arbitrarily chosen initial state $X_i^s(\mathrm{o}) = X_i(\mathrm{o}) = 0.5$. In Figure 1, $\overline{X}(n)$ is the *state vector* of the network and $\overline{\mu}^s$ is the *input-generating vector*. Note that depending on the nature of $\overline{\mu}^s$ (or its components μ_i^s) the network can be driven by coherent (periodic), partially

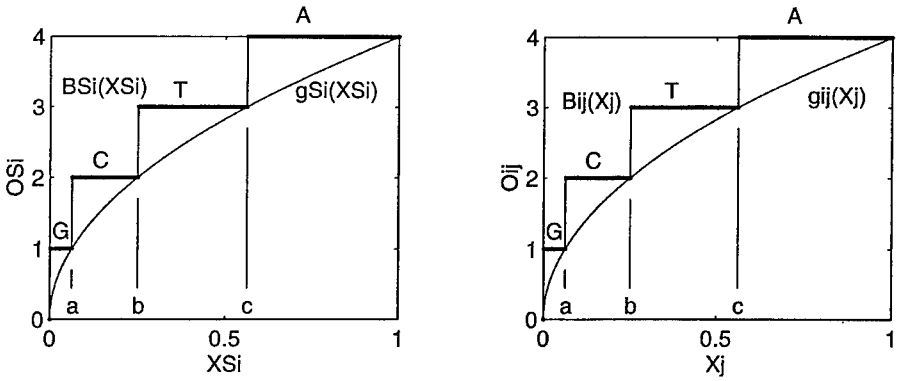

Figure 2. Nonlinear quantized (binned) coupling functions. (a) $B_i(X_i^s)$ between the sensory logistic elements and the network's PEs, and (b) $B_{ij}(X_j)$ between PEs.

coherent (partly periodic and partly chaotic), or chaotic input sequences (orbits) $B_i^s(X_i^s(n)) = B_i^s(n) = \mathrm{O}_i^s(n)$.

4. Simulation Results

In this section we summarize the results of numerical experiments carried out to date with the logistic net of Figure 1. To characterize the behavior of the parametrically coupled logistic net we have introduced the concept of *limit-set-diagram* (LSD). The LSD is a static representation of the state vector $\overline{X}(n)$ of the network, i.e., of the orbits $X_i(n)$, $i = 1, 2, \ldots, N$, of the PEs. It is formed by entering the values $X_i(n) \in [0, 1]$ visited by the post-transient orbit above each integer point $i = 1, 2, \ldots, N$ representing PE number taken as the abscissa of the diagram (see bottom row of Figure 3). The top row of Figure 3, shows three different input generating vectors $\overline{\mu}^s$. Those in (a) and (b) produce coherent stimulus vectors $X_i^s(n)$ and associated $B_i^s(n)$ because none of the components μ_i^s of the input generating vector are chaos inducing, i.e., $\mu_i^s < \mu_c = 3.56$. Here $\mu_c = 3.56$ is the critical value of the control parameter of a logistic map above which chaos is permitted. In both (a) and (b) the inputs to the network, $X_i^s(n)$ or $B_i^s(n)$, are therefore ordered and void of chaos. In (c) on the other hand $\overline{\mu}^s$ has chaos inducing components where $\mu_i^s > 3.56$. As a result, both $X_i^s(n)$ and $B_i^s(n)$ have few chaotic components ($93 \leqslant i \leqslant 100$) and the input to the network in this case is partially coherent.

The LSDs associated with each of these inputs are given in the bottom row of Figure 3. All these are seen to exhibit clustering wherein the PEs cluster into groups of identical orbits. The LSDs in (a) and (b) represent instances of the network converging to a periodic attractor of period-m and low dimension N_c, where $N_c \ll N$ is the number of clusters ($N_c = 6$ in (a) and $N_c = 7$ in (b)). Analysis of individual orbits of the PEs revealed that all those belonging to the same cluster have synchronized orbits i.e., identical orbits. Each cluster

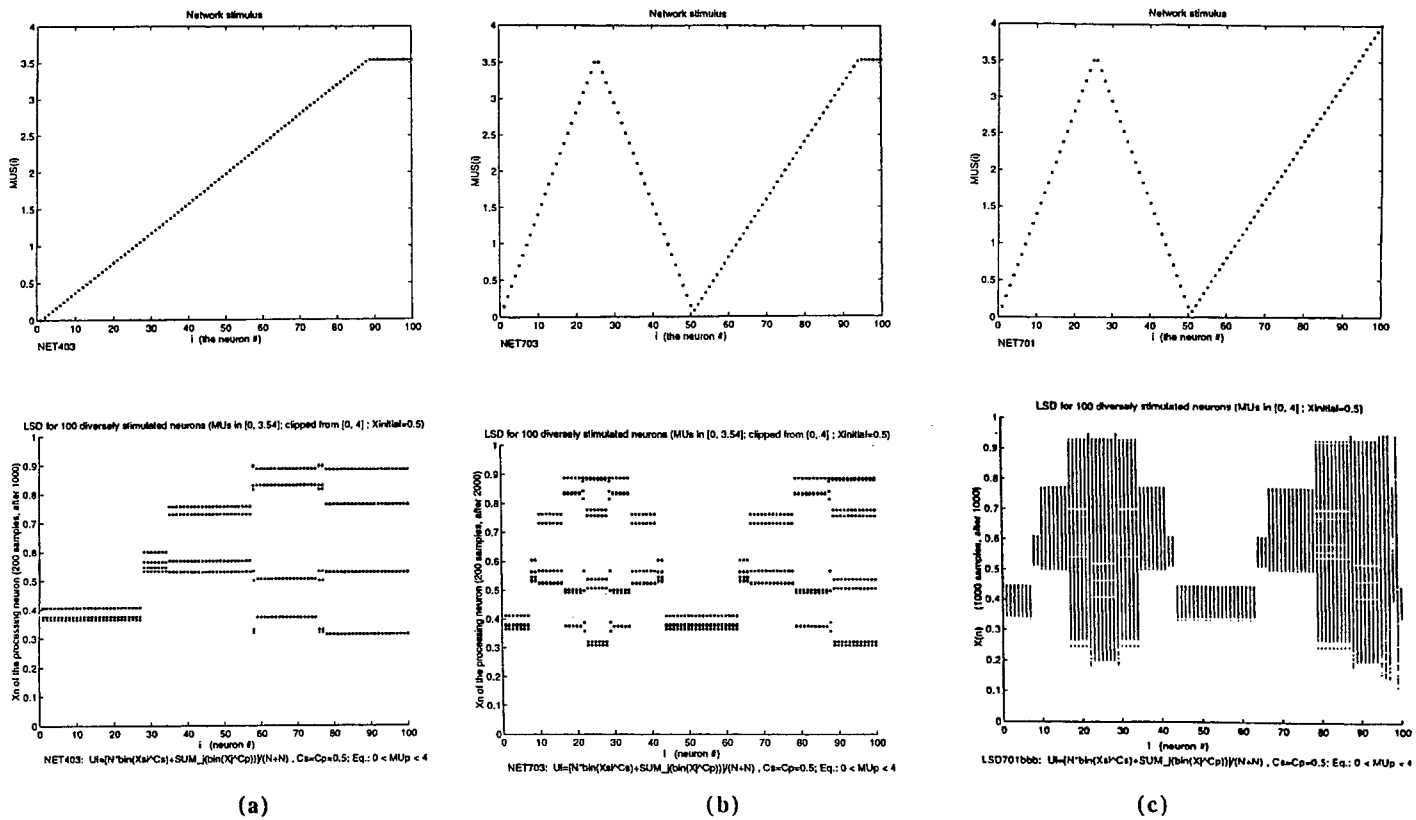

(a) **(b)** **(c)**

Figure 3. Limit set diagrams (LSDs) for a parametrically coupled logistic net of $N = 100$ logistic processing elements (LPEs), homogeneous binned coupling ($C_i^s = C_{ij} = 0.5$), and homogeneous initial states $X_i(\mathrm{o}) = X_0 = 0.5$. Three instances of input generating or feature vector $\overline{\mu}^s$ are shown in the top row and the LSDs they produce are shown in bottom row.

acts then as a single unit, i.e., like a "super-neuron". All six clusters are found to be phase-locked, in that they have distinct periodic orbits that are in fixed relative phase and of the same period – m. We found $m = 4$ in (a) and $m = 8$ in (b). Convergence to a periodic attractor is sudden following an erratic orbit interval of, for example, 1700 iterations for the case in (b). During the transient period, the network searches its state space for a "loss-region" in which it can collapse into a low-dimensional periodic attractor compatible with the constraints on the network namely the applied input and the coupling functions matrix. Similar analysis of PE orbits for the case in (c) shows the orbits do not converge to a periodic attractor even after observation over few thousand iterations, but appear instead to converge to a strange attractor by virtue of the distinct structure of the LSD in (c). In the LSD in (c), there appear to be a total $N_c = 10$ clusters out of which 8 consist of two or more PEs. Recall the input generating vector $\overline{\mu}^s$ in (c) had chaos inducing components for which $\mu_i^s > \mu_c = 3.56$. All this seems to suggest that when the input generating vectors considered here produce incoherent or partially coherent input patterns our net never converges to a periodic attractor but seems to converge instead to a strange attractor. One is tempted to hypothesize that convergence to a periodic attractor in dynamical nets is synonymous with recognition and classification of the input; while convergence to a strange attractor indicates lack of recognition because the input pattern presented to the net is not completely coherent (it contains incoherent (meaningless) components that do not correlate with other components of the feature vector (taken to be $\overline{\mu}_s$), and this prevents the network from linking the various parts of the feature vector into a coherent unit manifested by the convergence to periodic attractor. Close examination of the orbits $X_i(n)$ belonging to different clusters in this latter case shows they are not phase-locked because they do not exhibit any periodicity even over extended observation windows of 5000 iterations and more. This encourages us to suggest that phase-locking of clusters maybe used as mechanism of feature binding in dynamical networks such as the logistic net studied here.

5. Discussion

Dynamical nets, like the logistic net discussed here, show behavior consistent with the general idea in several cortical oscillations theories (von der Marlsburg, 1981, 1986; Abeles, 1982), and with the discovery of long-range temporal-correlation in cortical activity in cat and monkey (Eckhorn et al., 1988; Gray, 1989; Singer, 1993; Bosch et al., 1995; Engel et al., 1991(a), 1991(b); Murthy et al., 1992). At this stage of our work on dynamical nets we can make the following remarks that could be relevant to cortical dynamics and higher-level processing:

- Externally driven networks of parametrically coupled logistic processing elements constitute a computationally efficient setting for the simulation and study of dynamical neural networks and dynamical computing.
- Such networks compute with diverse attractors (point, periodic and chaotic (strange)) and are capable of bifurcating between attractors in the course of computation.
- In dynamical networks, bifurcation which is a sudden qualitative change in network behavior as a result of change in a control parameter or input, is a source of diversification and innovation that can lead to new solutions.
- Dynamical networks are capable of conducting transient chaotic search of their state space for attractors compatible with their input.
- The nonlinear (quantized or binned) coupling between processing elements used here allows rapid changes in the coupling between PEs to take place. It is introduced to loosely reflect the possibility that coupling between netlets is activity dependent and can change abruptly. We also find that binned coupling prevents fragmentation where the number of clusters (groups of synchronized PEs) becomes very large.
- The logistic network converges to a periodic attractor or to chaotic (strange) attractor depending on its input. When the input is coherent, the network collapses suddenly, following a transient search interval, to a low dimensional manifold, a periodic attractor associated with the particular input. When the input is incoherent or partially coherent it does not converge to a periodic attractor but seems to converge instead to a strange attractor.
- The dimension of the periodic attractor equals the number of clusters N_c, and $N_c \ll N$. It is as if the network partitions itself into a small number of subpopulations (clusters) with all "PEs" within a cluster having exactly the same orbit, i.e., have synchronized orbits. The clusters are phase-locked and each cluster can be viewed as a "super neuron".
- A small number of PEs (100 in the network simulated) can participate in a very large number of distinct convergent states depending on the constraints on the network (input and coupling between neurons). A relatively small net may be used therefore in the classification of a very large number of input patterns.
- When the input is incoherent we observe clustering with synchronicity within a cluster, but the clusters are not phase-locked.
- If we regard the input $\overline{\mu}^s$ to the dynamical (logistic) net considered here as a feature vector generator, then when the feature vector is coherent, because $\overline{\mu}^s$ has no chaos inducing components, i.e. (the input to the network will consist of correlated or meaningful components (features)), the network would converge to a periodic attractor performing thereby a feature binding operation. When the input is incoherent or partially coherent, meaning the components of the feature vector are not compatible with one another, the network con-

verges to a chaotic or strange attractor. The logistic net studied is capable therefore of performing a *feature-binding* or *feature-linking* operation.

- Coherence, phase-locking, and clustering of orbits provide the basis for a formalism for *neuroholography* (dynamic kinoform concept) because the state variable $X_i(n) \in [0,1]$, $i = 1, 2, \ldots, N$, of the network can be regarded as a normalized modulu 2π phase variable. Note kinoform is the term used in optics to describe a phase-only hologram.
- The form of the nonlinear coupling function between neurons, specifically the coupling factor C_{ij}, permits study and exploration of learning algorithms for dynamical networks possibly based on information theoretic measures of the orbits $X_i(n)$ like mutual information between orbits.

As stated earlier, the logistic net described and studied here is similar to Kaneko's *coupled map lattices* (Kaneko, 1993; Crutchfield and Kaneko, 1987). There are however three significant differences. One is the nonlinear and global nature of the coupling used here, two is the use of parametric coupling rather than diffusive coupling and three is the provision of auxilliary sensory elements for generating complex spatio-temporal input signals. Such provision of extrinsic input capability extends the scope of modeling applications of parametrically coupled nets of logistic or, other bifurcation processing elements, beyond those listed above. For example, one can study the behavior of such nets when the parameter ε in Equation (1) is made to slowly decay exponentially in time in order to pass the control over network dynamics from initially extrinsically dominated control to eventually completely intrinsic control. The effect of the extrinsic input in this scenario is to conduct the network to specific region of its state-space when all the while it is being gradually released to entirely intrinsic control. Such behavior maybe plausible in biological networks (Freeman, 1995) and may also be relevant to the development of learning algorithms for dynamical networks.

Acknowledgement

This work was supported by The Office of Naval Research under grant no. N0001-94-1-093 P01. The author wishes also to acknowledge valuable discussions with Emilio del Moral Hernandez and Andrew Baek.

References

1. Abeles, M.: 1982, *Local Cortical Circuits*, Springer, New York. Also, Corticonics: Neural Circuits of the Cerebral Cortex, Cambridge Univ. Press, NY, 1991.
2. Annios, P. A. et al.: 1970, *J. Theoretical Biology* **26**, 121–148.
3. Bertille, J. M. and Perez, J. C.: 1990, in: *Proc. IJCNN'90*, L. Erlbaum Associates Publishers, Hillsdale, NJ, pp. 361–364.
4. Bosch, M., Bauer, R., and Eckhorn, R.: 1995, *European Journal of Neuroscience* **7**, 86–95.
5. Crutchfield, J. and Kaneko, K.: 1987, in: *Directions in Chaos*, Vol. 1, World Scientific Publishing Co., Singapore, pp. 272–353.
6. Eckhorn, R.: 1988, *Biological Cybernetics* **60**, 121–130.

7. Edelman, G. M.: 1987, *Neural Darwinsim: The Theory of Neuronal Group Selection*, Basic Books Inc. Publishers, New York.
8. Engel, A. K., König, P., Kreiter, A. K., and Singer, W.: 1991, *Proc. National Academy Sciences USA* **88**, 6048–6052.
9. Engel, A. K., König, P., Kreiter, A. K., and Singer, W.: 1991, *Science* **252**, 1177–1179.
10. Farhat, N. and Hernandez, E. del Moral: 1996, Recurrent nets with recursive processing elements: Paradigm for dynamical computing, in: *SPIE*, Vol. 2324, SPIE, Bellingham, Washington, pp. 158–170.
11. Farhat, N. and Hernandez, E. del Moral: 1995, in: *From Natural to Artificial Neural Computation*, Springer, Berlin, pp. 215–222.
12. Farhat, N., Lin, S.-Y., and Eldefrawy, M.: 1994, Complexity and chaotic dynamics in a spiking neuron embodiment, in: *Adaptive Computing, Mathematics, Electronics, and Optics, SPIE*, Bellingham, Washington, pp. 77–88.
13. Freeman, W. J.: 1995, *Societies of Brains*, LEA Associates Publishers, Hillsdale, NJ.
14. Gray, C. M. et al.: 1989, *Nature* **338**, 334–337.
15. Harth, E. M. et al.: 1970, *J. Theoretical Biology* **26**, 93–120.
16. Hilborn, R. C.: 1994, *Chaos and Nonlinear Dynamics*, Oxford Univ. Press, New York.
17. Kaneko, K.: 1993, in: K. Kaneko (ed.), *Theory and Applications of Coupled Map Lattices*, Wiley, New York, pp. 1–49.
18. Marlsburg, von der C.: 1981, The correlation theory of brain functions, Internal Report 81-2, Max-Plank Institute for Biophysical Chemistry, Götingan, FRG.
19. Marlsburg, von der C.: 1986, *Biological Cybernetics* **54**, 29–40.
20. Murthy, V. N. and Fetz, E. E.: 1992, *Proc. National Academy of Sciences, USA* **89**, 5670–5674.
21. Perez, J. C. and Bertille, J. M.: 1989, in: *Proc. INNS First Annual Meeting*, Boston, September 1989, p. 121.
22. Singer, W.: 1993, *Annual Review of Physiology* **55**, 349–374.
23. Usher, M., Schuster, H. G., and Neibur, E.: 1993, *Neural Computation* **5**, 370–586.
24. Vreeswijk, van C. and Sompolinski, H.: 1976, *Science* **274**, 1724–1726.
25. Wennekers, T. and Pasemann, F.: 1996, *International Journal of Bifurcation and Chaos in Applied Sciences and Engineering* **6**, 2055–2067.
26. Wennekers, T., Sommer, F., and Palm, G.: 1995, in: H. Hermann, D. Wolf and E. Pöppel (eds), *Supercomputing in Brain Research: From Tomography to Neural Networks*, World Scientific, Singapore.